2016

A Model of the Effects of Deforestation on Local Climate in the North Cascades

Monica R. H. Jasper

A Model of the Effects of Deforestation on Local Climate in the North Cascades

Monica R. Hanson
University of Denver Department of Geography

Capstone Project

For

Master of Science in Geographic Information Science

March 10, 2016

Abstract

Changes in areal extent of land cover types may lead to alterations in the surface energy budget that contribute to anthropogenic climate forcing. This study examines the effects of deforestation in the Cascade Range on local temperature. Temperature sensors were installed in 14 forest stands, taking measurements for one year. Estimated tree age, circumference, and species were recorded to calculate stand density index. Satellite imagery was used to calculate shade fraction from spectral mixture analysis, which is a proxy for canopy structure and density. These data were used to construct seasonal cycles of temperature to model variation with stand density and elevation. Maximum daily temperatures were 3.6°C higher in clearcut than mature forests in summer and 2.6°C higher in winter.

Keywords

deforestation, remote sensing, climate modeling, spectral mixture analysis, surface air temperature, stand density, topographic shade, GIS, Washington

Table of Contents

Introduction..... 1

Background..... 5

Deforestation Effects on Radiant Energy Budget..... 5

Biophysical and Biogeochemical Factors..... 6

Study Area..... 11

Design and Implementation..... 11

Project Design..... 11

Field Methods..... 12

Data Sources..... 13

Site Characteristics..... 15

Shade Fraction..... 15

Surface Temperature Model..... 18

Pre-Anthropogenic Model..... 20

Results..... 22

Raw Temperature Data..... 22

Shade Fraction..... 24

Surface Temperature Model..... 26

Pre-Anthropogenic Model..... 29

Table of Contents (cont.)

Discussion..... 32

Areas for Future Research..... 34

Acknowledgements..... 35

References.....36

Introduction

The Cascade Range of western North America is a heavily forested mountain range with an active timber industry. As a result of clearcutting, North Cascades forests are currently a patchwork of young trees of various ages, with many stands of old growth forests as well. In 2008, I was a field assistant supporting the M.S. thesis project of Lyndsey Roth near the Mt. Adams Wilderness in Gifford Pinchot National Forest (Figure 1). That study evaluated whether temperature significantly differed in clearcut versus old growth forests. Sensors were placed in forest stands to automatically collect climate measurements every 15 minutes from July 20, 2008, through September 17, 2008. That study concentrated on August out of a motivation to understand the effects of clearcutting on near surface temperatures that may affect nearby glacier melt rates in the area. O'Neal et al. (2009 and 2010), Goldstein (2008), and Roth (2009) concluded that the presence of clearcuts generated a regional average increase of 0.7°C in daily maximum temperature over the study area. They attributed this difference to the greater efficiency of forested areas, as compared to clearcut areas, in transferring latent heat (water vapor) and sensible heat (heat perceived as temperature) to the atmosphere, primarily through the increased direct coupling of the surface to the air when the wind can blow through the trees. In August 2012, temperature sensors were set up in the

study area and left until August 2013 in order to observe a full year of climate effects.

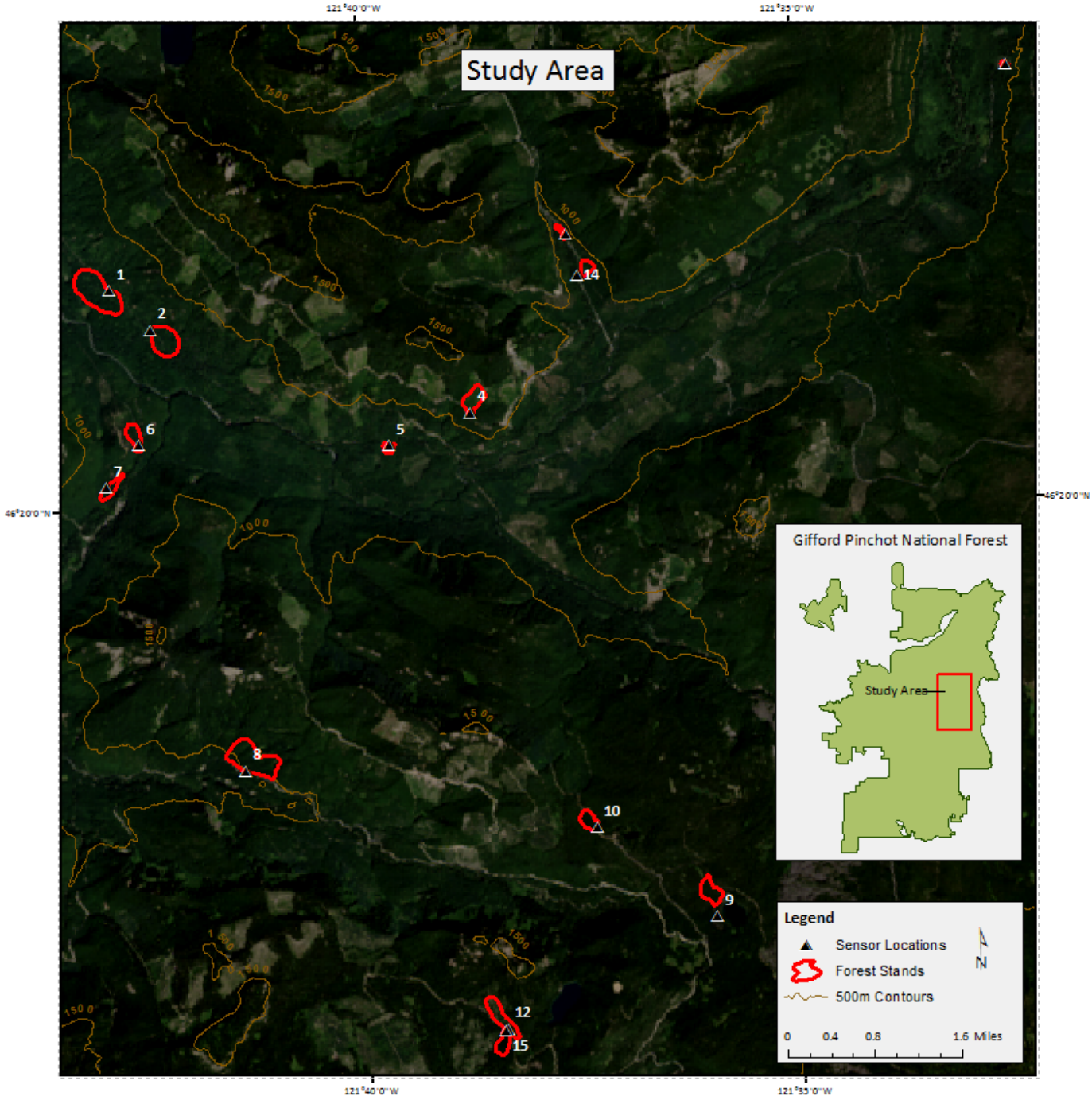

Figure 1. Study area within Gifford Pinchot National Forest, Washington. Forest stands and sensor locations were digitized over Landsat 8 imagery.

The objective of this project is to determine not just whether land-cover changes contribute significantly to anthropogenic climate forcing, but also how they vary seasonally. By modeling temperature changes throughout the year in several forest stands of various ages, it is possible to record the influence that deforestation has on local temperature. Due to the importance of a strong albedo as a significant factor in causing net warming effects from deforestation at boreal latitudes, we will examine how winter and year-round conditions affect the local climate of western Washington in clearcut and mature growth forests. Specifically, this research seeks to answer:

- Are there significant differences in maximum surface air temperature between clearcut and mature growth forest stands during winter conditions?
- Does deforestation cause a net cooling, warming, or negligible change in the annual and seasonal radiation energy budget?
- Does the effect of increased albedo from snow cover in clearcut stands outweigh the seasonal (or annual) increase in surface air temperature in the study area?
- What is the temperature anomaly between pre-anthropogenic and current forest conditions, and how does this anomaly change throughout the year?

For this capstone project, I have modeled the year-round effect of deforestation on local climate in the Gifford Pinchot National Forest study area, accounting for various stand parameters that affect climate, and paying particular attention to snow cover, which could not be modelled in the previous study.

Previous studies have found that deforestation increases temperature in tropical climates and decreases temperature in boreal climates where snow's albedo effect is greater (Bonan, 2008; Houspanossian et al., 2013; Li et al., 2015). In Washington's temperate climate, deforestation should increase local temperature during the summer months and decrease local temperature during winter snow. We expect that the overall effect of deforestation on local climate in this region will be a minor, but noticeable warming.

Deforestation has generally been assumed to have a regional effect on climate, with theories about its influence on climate going back centuries (Pearson, 1914; Fritts, 1961; Hornbeck, 1970; McCaughey, 1985; Carlson & Groot, 1997; O'Neal et al., 2010). The precise effects of deforestation vary from region to region, and will vary locally at different times of year. The data available for this project should shed light on seasonal and annual climate variations, and provide a model that can assist with better land management and forestry practices in the Cascades region.

Background

Deforestation Effects on Radiant Energy Budget

Over the last century, numerous studies conducted in actively logged terrains have found that daily maximum near-surface temperatures in mid-latitude mature and old-growth forests are lower than adjacent clearcut and young regrowth sites (Pearson, 1914; Fritts, 1961; Hornbeck, 1970; McCaughey, 1985; O'Neal et al., 2009). The seasonal energy balance resulting from forest cover reduction at temperate latitudes may remain unchanged, however the near-surface daytime and nighttime temperatures typically increase in a clearcut site relative to a forested site, which can cause significant biophysical and biogeochemical changes in the radiant energy budget (Hornbeck, 1970; Bonan, 2008; Lee, 2011; Houspanossian et al., 2013; Li et al., 2015).

Deforestation is widespread, and until recently, heavily unchecked, as mature and old-growth forest land was replaced by crops and grasslands for agriculture and clearcut or young, successional regrowth in areas of timber harvest. Effects in reduction of forest-cover have been studied at global scales to better understand how anthropogenic land cover change is altering climate. Several studies have examined these global effects using data from tropical, temperate, and boreal forests around the world, which have resulted in marked differences in northern and southern hemisphere forests stratified by latitude (Lee et al., 2011; Zhang et al., 2014; Li et al., 2015).

Boreal forests show strong warming in winter and moderate cooling in summer, and result in a net warming annually (Li et al., 2015). At high latitudes above 35°N to 50°N, deforestation leads to a significant increase in albedo from exposed snow cover that has a large cooling effect (Lee et al., 2011; Houspanossian et al., 2013; Zhang et al., 2014; Li et al., 2015). The opposite is true for tropical forests, where biogeochemical processes outweigh the change in albedo, so tropical deforestation has a net warming effect (Houspanossian et al., 2013; Li et al., 2015). Large-scale trends toward both net cooling and warming have been observed for temperate deforestation, due in part to negligible temperature differences, high variability in the carbon balance, and uncertain biophysical processes. Since temperate forests are particularly vulnerable to land use changes, previous studies have focused on examining the climatic effects of mid-latitude forest-cover change at local scales (O'Neal et al., 2010).

Biophysical and Biogeochemical Factors

There are many complex biophysical and biogeochemical factors at work that have differing roles in how deforestation affects local climate. The net climate benefit of forests fluctuates with diurnal cycling, seasonally, and with latitude (Li et al., 2015; Houspanossian et al., 2013; Lee et al., 2011; Zhang et al., 2014). The physical properties associated with replacing temperate forests with cropland, grassland, and clearcut sites have a significant impact on the energy budget. Biogeophysical processes include

the moisture cycle, which encompasses evapotranspiration, land use, surface roughness, vegetation dynamics, and precipitation, and effects of radiation, which include albedo and the partition between latent and sensible heat.

Spatial heterogeneity is strongly affected by changes in land cover, which can cause either a warming or cooling effect depending on the relative influence of evapotranspiration and radiation. Higher canopy roughness and aerodynamic conductance of forests compared with herbaceous vegetation translate into a higher capacity to transfer latent and sensible heat into the surrounding atmosphere, and cools surface temperature through evapotranspiration (Houspanossian et al., 2013). Replacement of forest canopies with cropland results in increased outgoing longwave radiation, and a net loss of energy. Regions with high atmospheric moisture during spring and summer experience more cloudiness, have decreased boundary layer height, net radiation, and sensible heat flux, and have increased latent heat flux, rates of infiltration, and soil water. Intensive agriculture reinforces these signals, and individual months show even larger, statistically significant differences in precipitation from land use practices (Bonan, 1997).

Water stored in soil regulates latent heat flux (Fritts, 1961; Klingaman et al., 2008). When soil moisture and the vapor pressure deficit are high, a portion of the energy is dissipated through evapotranspiration. Coupled with reduced incoming solar radiation from cloudy weather, evaporation absorbs

heat at the forest floor and results in a decrease in air temperature (Fritts, 1961). Forest and agricultural land have similar surface radiative temperature when soil is moist, but during periods of drought, agricultural land can warm 13°C more than forest cover due to the deep roots of trees which can access deeper groundwater reservoirs (Bonan, 2008). Carlson & Groot (1997) also observed seasonal variations in soil temperature that increased with forest canopy size. The difference in soil temperature between open and canopied land cover was greatest early in the season, and diminished as regeneration of shrubs, herbs, and grasses filled in openings.

Klingaman et al. (2008) found strong diurnal and seasonal temperature variation related to deforestation in a mesoscale atmospheric model. During summer, air temperature increased by more than 1.5°C within the northern Pennsylvania study area. This effect was most apparent at night, likely due to the return of heat stored within the soil from the day and a reduction in atmospheric boundary mixing. In August, deforestation redistributed the surface energy budget most, decreasing latent heat flux by 60 W/m^2. McCaughey (1985) also observed greater reflectance of solar radiation and higher daytime surface temperature in clearcut areas. Differences between daytime and nighttime summer air temperature were much greater in clearcut compared with forest regions due to shortwave irradiance (Carlson & Groot, 1997). Within their southern Ontario study area, average maximum to minimum differences were 17.1°C on clearcut

land, but decreased to 10.1°C under forest canopy. The magnitude of night warming, which was highest in forests at mid-latitudes, was outweighed by the dominant daytime cooling effect (Li et al., 2015). Although daytime land surface temperature had a greater role in daily average temperature, nighttime surface temperature had the ability to enhance, counteract, or even reverse the daytime effect, leading to a weak daily cooling of approximately 0.27°C in the northern hemisphere (Li et al., 2015).

The biophysical effects discussed so far primarily point to forests having a cooling effect, which is most pronounced in summer. Albedo is an important exception, which suggests that forests have a warming effect during winter. Surface albedo increases with deforestation, and this effect is most pronounced at higher latitudes where snow cover in open areas causes high reflectance and subsequent cooling. A substantial increase in albedo is observed during winter from snow cover, reinforced by a land albedo-sea ice feedback, and has the potential to cool the Earth's surface at higher latitudes by altering biophysical processes (Bonan, 1992; Lee et al., 2011). Houspanossian et al. (2013) estimate a mean radiative increase in 3 W/m^2 in temperate regions and 20 W/m^2 in boreal areas from forestation. However, this study emphasizes that these values do not account for the large spatial variability that biogeochemical and biophysical effects can have depending on localized land-use changes.

Forests strongly influence the biogeochemical cycles; primarily the carbon cycle, but also the nitrogen and phosphorous cycles. Changing tree cover alters atmospheric carbon dioxide concentrations (Li et al., 2015). Nitrogen is pulled from the atmosphere and soil for leaf growth in deciduous forests, so deforestation causes a large nitrogen spike. Bonan (2008) examined albedo, evapotranspiration, the carbon cycle, and the alteration of forest-atmosphere coupling through land use and vegetation dynamics. Inclusion of biogeochemical processes in energy budget models is new and emerging, however biophysical forcings tend to be more influential in changing climate.

There are two driving, competing effects of deforestation—evapotranspiration and albedo—which are strongly influenced by rain, snow, and other climate factors (Bonan, 1997; Li et al., 2015). The strength of albedo warming increases with latitude, and the strength of evapotranspiration cooling decreases with latitude. "Higher albedo with loss of forest cover could offset carbon emission so that the net climatic effect of temperate deforestation is negligible, or reduced evapotranspiration with loss of trees could amplify biogeochemical warming. The future of temperature forests and their climate services is highly uncertain" (Bonan, 2008). There is more to learn about the relative strength of each of these forcings in determining radiant energy budget at temperate latitudes.

Study Area

The Cascade Range of Washington and northern Oregon consists of the older, heavily eroded Western Cascades and the younger High Cascade stratovolcanoes. This region is marked by high levels of precipitation, mild temperatures, expansive forests, and extensive timber management. This study was conducted in a 15 km square area of the Gifford Pinchot National Forest, Washington, approximately 6 km northwest of Mt. Adams, located between 46.26°N to 46.40°N latitude, and 121.73°W to 121.53°W longitude (Figure 1). Forests within the study area are a heterogeneous mixture of managed and native stands with saplings to mature growth trees estimated to be several hundred years old (USDA, 1999). Stands within the study area occur over relatively steep terrains with approximately 20° to 30° slopes and elevations ranging from 600 m ASL to 1350 m, and are predominantly composed of Douglas fir, pacific silver fir, grand fir, western hemlock, and mountain hemlock species (Little, 1980).

Design and Implementation

Project Design

The goal of this project is to better understand temperature differences in forests of different elevations, stand densities, and canopy structures. Numerous studies have observed that daytime and summer daily maximum temperatures are higher in clearcut or open areas than in adjacent mature forests (Fritts, 1961; Hornbeck, 1970; McCaughey, 1985;

O'Neal et al., 2009). Research in forests adjacent to our study area reported 5°C to 7°C differences in average daily maximum temperatures of mature forests and logged terrain (Barg & Edmonds, 1999; Heithecker & Halpern, 2006).

Field Methods

This study was focused on developing a better understanding of factors affecting local temperature differences, such as stand density, elevation, canopy structure, and seasonal changes in lapse rate. O'Neal et al. (2010) used USDA forest inventory data, topographic maps, and satellite imagery to direct placement of temperature sensors in 14 forest stands, selecting for a variety of densities, ages, and canopy structures. Hobo Pro V2 temperature/humidity data loggers were placed approximately 1 m above the land surface and at least 50 m inside each forest stand to prevent potential boundary effects, and air temperature was measured at 15-minute intervals from August 20, 2012, to August 16, 2013. In 2008, I assisted with collecting field measurements for a prior study (Roth, 2009), which included tree circumference, species composition, and species distribution within 10 m by 10 m representative areas at each site location. Temperature data was taken for two additional stands in 2012, referencing stand density index (SDI) measurements taken in 2008.

Data Sources

Data acquisition involved a mixture of primary climate, location, and stand density data collected in the field, satellite photos, and digital image processing to determine site parameters such as elevation, slope, aspect, topographic relief, and forest shade for the climate model (Table 1).

Sensor locations were recorded in the WGS 1984 UTM Zone 10 N coordinate system using a Magellan eXplorist handheld GPS unit with 4 m accuracy. Forest stand areas surrounding each sensor were delineated in ArcGIS (by ESRI) with high-resolution NAIP (National Agriculture Imagery Program) orthophotos, and cross-checked against Google Maps, Landsat 8 imagery, and site maps from Roth (2009).

Sensor	Latitude	Longitude	Elevation (m)	Slope	Aspect	Shade Fraction	Stand Density Index	Estimated Age Range
1	46.36	-121.72	626	50	224	0.6359	1095	50-75
2	46.36	-121.71	677	51	230	0.5007	862	100-125
3	46.39	-121.54	964	75	255	0.2920	338	0-25
4	46.35	-121.65	1152	64	223	0.5808	341	25-50
5	46.34	-121.66	744	83	233	0.0000	156	0-25
6	46.34	-121.71	725	59	66	0.6749	1118	100-125
7	46.33	-121.71	722	47	145	0.6771		75-100
8	46.30	-121.69	1033	49	204	0.6083		50-75
9	46.28	-121.60	1344	57	213	0.5302	864	50-75
10	46.29	-121.62	1305	59	97	0.5803	1234	100-125
12	46.26	-121.64	1294	73	223	0.2812	137	0-25
13	46.37	-121.63	950	85	131	1.0000	1809	125-150
14	46.36	-121.62	956	53	256	0.5709	484	25-50
15	46.26	-121.64	1286	46	242	0.6368	1903	125-150

Table 1. Summary of forest stand information. Sensor locations are in coordinate system WGS 1984 UTM 10N. Elevation, slope, and aspect were calculated from the DEM as averages over the forest stand area. Shade fraction was calculated in ENVI from Landsat 8 imagery and is correlated

with the 2008 stand density index values taken from Roth (2009). Age ranges were estimated from site photos and stand density.

To allow for easier numerical analysis, temperature measurements were interpolated from the Hobo Pro V2 data loggers into an equidistant time series of 100 points per day (as opposed to 96) that are precisely the same time for each sensor.

Satellite imagery was acquired using the U.S. Geological Survey's EarthExplorer web map, which provides data collected from the Earth Resources Observation and Science Center (EROS). EROS Landsat images were orthorectified, and available on a 16 day frequency. The appropriate Landsat scene for our study area falls in path 046 and row 028. Imagery encompassing the entire duration of the study period were collected. However, extensive cloud cover during the wet season limited usability. The scan line corrector instrument on the Landsat 7 satellite failed in 2003, producing an artificial zig-zag pattern on all subsequent imagery that is not conducive to large-scale image processing. Fortunately, the Landsat 8 satellite was launched during this study, with better images (working scan line corrector) of comparable resolution, frequency, location, and band compositions, which were available starting in April 2013. Landsat 8 imagery collected on August 20, 2013 (LC80460282013232) was used for the bulk of analysis. Atmospheric corrections and additional preprocessing techniques were not deemed necessary for this imagery because of the dry

clear summer skies typical of this region. An ASTER (Advanced Spaceborne Thermal Emission and Reflection Radiometer) global digital elevation model (DEM) was also acquired from EarthExplorer (ASTGTM2_N46W122_dem) to obtain hypsometric data for the study area.

Site Characteristics

Several parameters for the climate model were derived from the ASTER GDEM and Landsat 8 imagery. Using ArcGIS, the GDEM and imagery were transformed to the same spatial coordinate system (WGS 1984 UTM Zone 10 N), georeferenced, clipped to the study area, and resampled to have the same number of rows, number of columns, and cell size (resolution). A composite of bands 2, 3, and 4 was created to produce a natural color image, and bands 3, 4, and 5 were combined to produce a near-infrared image, showing differences in vegetation health. Slope, aspect, and elevation were calculated from the GDEM. Each raster was extracted by forest stand areas, and the mean values of each stand were calculated.

Shade Fraction

Shade fraction has been shown to be a reliable proxy for stand density in climate models (Goldstein, 2008; Roth, 2009). Other common remote sensing techniques for estimating forest structure include normalized difference vegetation index (NDVI) and soil-adjusted vegetation index

(SAVI), however shade fraction from spectral mixture analysis (SMA), after topographic shade is removed, has been shown to provide a better proxy for detecting stages of regrowth in forests based on a variety of physical properties and canopy structures (Shimabukuro et al., 1998; Sabol et al., 2002; O'Neal et al., 2009). Old-growth forests have more shade and shadow variations from differences in tree height and stand density, whereas young stands have little to no shade because trees are of a similar height during the initial stages of regrowth or entirely absent in fresh clearcuts.

The shade fraction calculation required use of the remote sensing software ENVI (by Exelis Visual Information Solutions) for image processing. Landsat 8 bands 2 through 7, the visible light, near infrared, and shortwave infrared wavelengths, were stacked and used as the base raster layer for spectral mixture analysis. To remove topographic shade (shadows created by slopes), shaded relief of the GDEM was calculated using the sun elevation and sun azimuth values of the Landsat 8 scene. Ideally, the shaded relief image can be subtracted from each band, and the restacked image should represent the stacked base layer with shade removed (Kane et al., 2008; Gu & Gillespie, 1998). Instead, proper and full removal of topographic shade was one of the more challenging aspects of this project.

Subtracting the hillshade from each band tended to overcorrect for shade, leaving previously darkened hills abnormally light. Subsequently, subtraction of a proportion of hillshade was attempted, and through trial and

error, the proportion that best removed shade for each band was applied. Visual inspection of successful shade removal was especially difficult to assess with the darker bands 2, 3, 4, and 7. After the individually shade-corrected stands were stacked, topographic shade was once again evident. In order for the SMA to work, band calculations needed to be consistent, so a single 'best-fit' proportion of topographic shade removal was assessed for all bands. Ultimately, subtraction of 5 percent hillshade was best for consistent removal of topographic shade across all bands, given $b1-(b2\cdot 0.05)$, where $b2\cdot 0.05$ is the proportion of hillshade being removed from band $b1$. The stacked bands reveal some lingering shade effects, but the majority of diffuse shade and topography shadows were removed.

SMA assumes the reflectance of pixels results from variations in the proportion of different landscape elements, and is used to estimate the composition of individual pixels. This requires that land cover be classified, which can be performed by automatically generating classes with the unsupervised Classification workflow, or through manual creation of Regions of Interest (ROI).

ROIs were established by creating new vector layers, and digitizing polygons around pixels representative of primary land cover types in the study area: water, bare rock, spare vegetation, dense vegetation, and snow

cover. Each vector was saved as a shapefile, then jointly converted into a five part ROI with the shade-removed stacked bands as the base layer.

The Linear Spectral Unmixing workflow was used to perform SMA, using the ROI for the Endmember Collection inputs, and applying a unit-sum constraint to a weight of 1 to generate unmixed endmembers. Finally, shade fraction is calculated from:

$$D = \frac{b1}{b1 + b2 + b3 + b4 + b5}, \quad (1)$$

where $b1$ is the water spectra, used as a proxy for shade, and $b2$, $b3$, $b4$, and $b5$, are the remaining spectral endmembers.

Using ArcGIS, the shade fraction image was extracted by forest stand boundaries, and the zonal statistics tool was used to determine mean shade fraction values in each stand. Results were normalized using the raster calculator to between 0 and 1, which represent relative changes in shade, and subsequently canopy density.

Surface Temperature Model

The precursor studies to this capstone project (Roth, 2009; O'Neal et al., 2009; O'Neal et al., 2010) developed a model that describes how temperature changes with forest characteristics. This model was based on the ability of shade generated by SMA to be a proxy for canopy density,

where high shade results from mature, dense forests, and less shade is produced in bare or young regrowth stands. The temperature model was developed to broadly understand how annual and seasonal local climate variations are affected by deforestation.

This model is based on two assumptions. The first is that temperature *T* at any given elevation is partially a function of lapse rate in an alpine setting:

$$T = T_0 + \Gamma \cdot (z - z_0) \text{ ,} \tag{2}$$

where T_0 is the temperature at a reference elevation, z_0 (743 m for this model based on a particular clearcut), z is the land surface elevation at a given stand, and Γ is the lapse rate, representing the change in temperature with elevation. The most appropriate environmental lapse rate was determined by minimizing the root mean squared error and determining the least-squares fit using the field-measured temperature data.

The second assumption is that the primary forcings determining near-surface temperature within a stand at a given elevation are stand density and canopy structure, for which shade fraction is a proxy. This temperature anomaly can be expressed as:

$$T_a = D \cdot \Delta T, \tag{3}$$

where D represents the percent shade for a given stand, obtained from the SMA shade fraction image, and ΔT is the monthly maximum temperature range between a mature forest and a clearcut. This anomaly relates temperature to the amount of shade observed in satellite imagery, where ΔT is calculated from the difference between measured temperatures in a clearcut stand with proportionally zero shade, and from an old-growth stand characterized with a shade fraction of one (100 percent shade). Combining equations (1) and (2) produced a modeled near-surface temperature that accounts for the effects of the environmental lapse rate around elevation changes and stand density:

$$T_D = T_0 + \Gamma(z - z_0) - D \cdot \Delta T. \quad (4)$$

The monthly average of daily high near-surface temperatures measured in 14 stands over the course of a year were used to examine the annual and seasonal reliability of the model. Monthly averages of daily maximum high temperatures were of particular interest because maximum temperatures most greatly influence glacial melt, and thus have a greater impact on climate forcings.

Pre-Anthropogenic Model

We modeled the difference between pre-anthropogenic and present-day temperatures over the study area using the assumption that pre-anthropogenic vegetation in the North Cascades was predominantly

mature forest. NDVI was calculated using the difference in the near-infrared and red spectra (Landsat 8 bands 5 and 4) as a proxy for terrain that is naturally vegetated, and areas such as bare rock, water, snow that are not (Figure 2). The vegetated and bare areas were classified and assigned values of 1 and 0, respectively. For NDVI values assigned as 0, we assumed that the shade fraction did not change, since bare rock and water did not change significantly as a result of human activity within this study area. If NDVI was not assigned a value of 0, the shade fraction was subtracted from 0.8, which Roth (2009) used as a proxy for maximum shade.

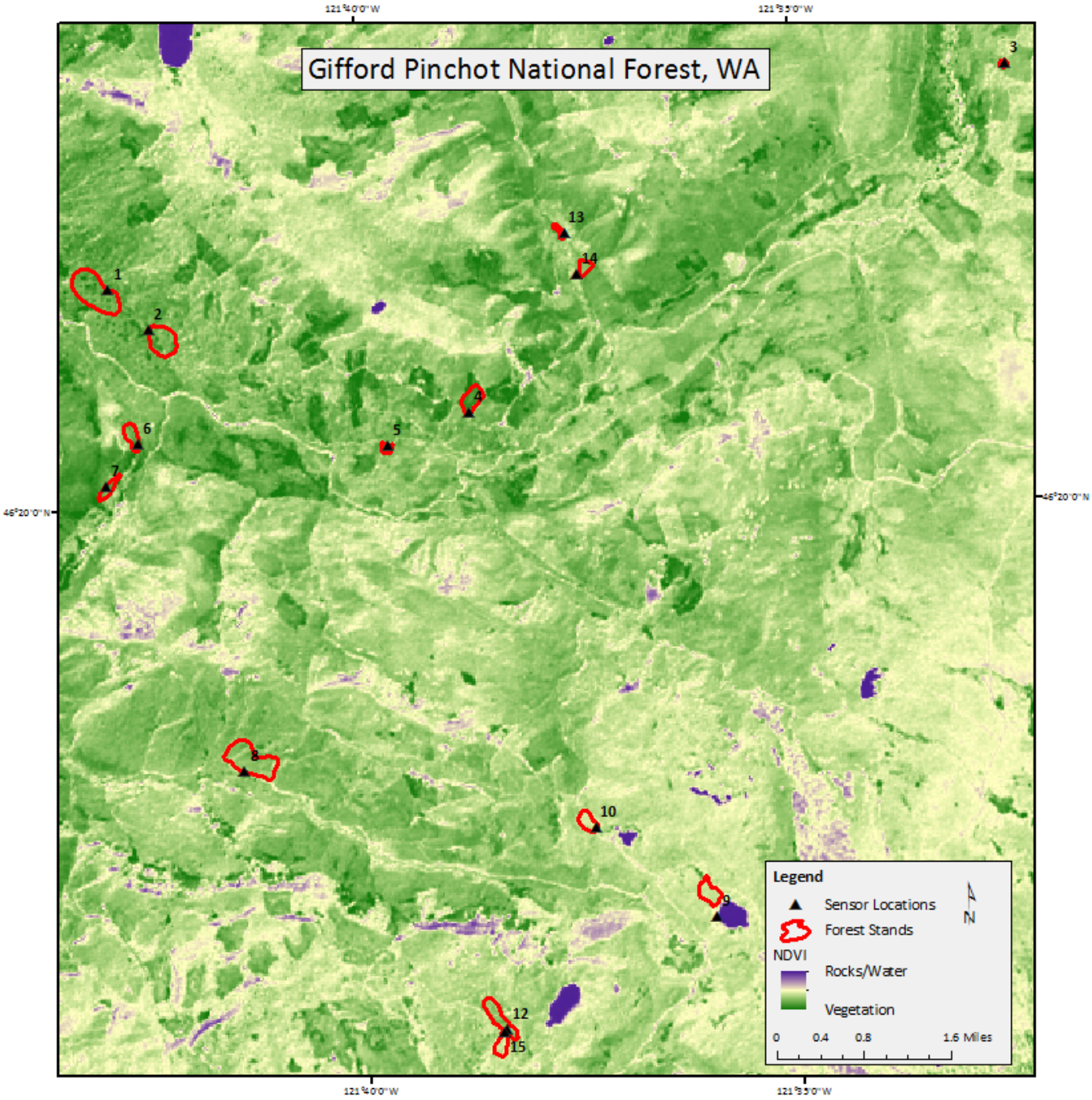

Figure 2. Normalized Difference Vegetation Index (NDVI) for study area, showing high vegetation areas in dark green, moderately vegetated areas in yellow, and areas with low vegetation, such as rocks and water, in purple.

The result of this calculation is the difference in shade fraction ΔD between the pre-anthropogenic and current landscape. The sum of the difference in shade fraction pixels was compared with the sum of current shade fraction pixels, and this proportion was multiplied by the monthly temperature anomaly to produce the expected difference in temperature between pre-anthropogenic and current landscapes.

This temperature difference is closely approximated by equation 3. The effect of elevation represented by equation 2 was not considered in the model under the assumption that significant tectonic activity did not occur from the pre-anthropogenic landscape to the present.

Results

Raw Temperature Data

In total, 36,100 temperature measurements were evaluated for each of the 14 stands. Annual mean temperatures for each stand ranged from 3.94°C to 8.26°C, which correspond with the highest elevation (stand 9 at 1343 m) and lowest elevation (stand 1 at 625 m) endmember sites, respectively. This suggests that the environmental lapse rate from changes in elevation is a significant factor for mean temperature. The overall maximum temperature for the study duration was 36.98°C, again found at stand 1 with the lowest elevation, which had moderate canopy density, and the overall minimum temperature of -16.33°C was found at stand 3.

The monthly averages of daily maximum temperatures show marked seasonal fluctuations (Figure 3).

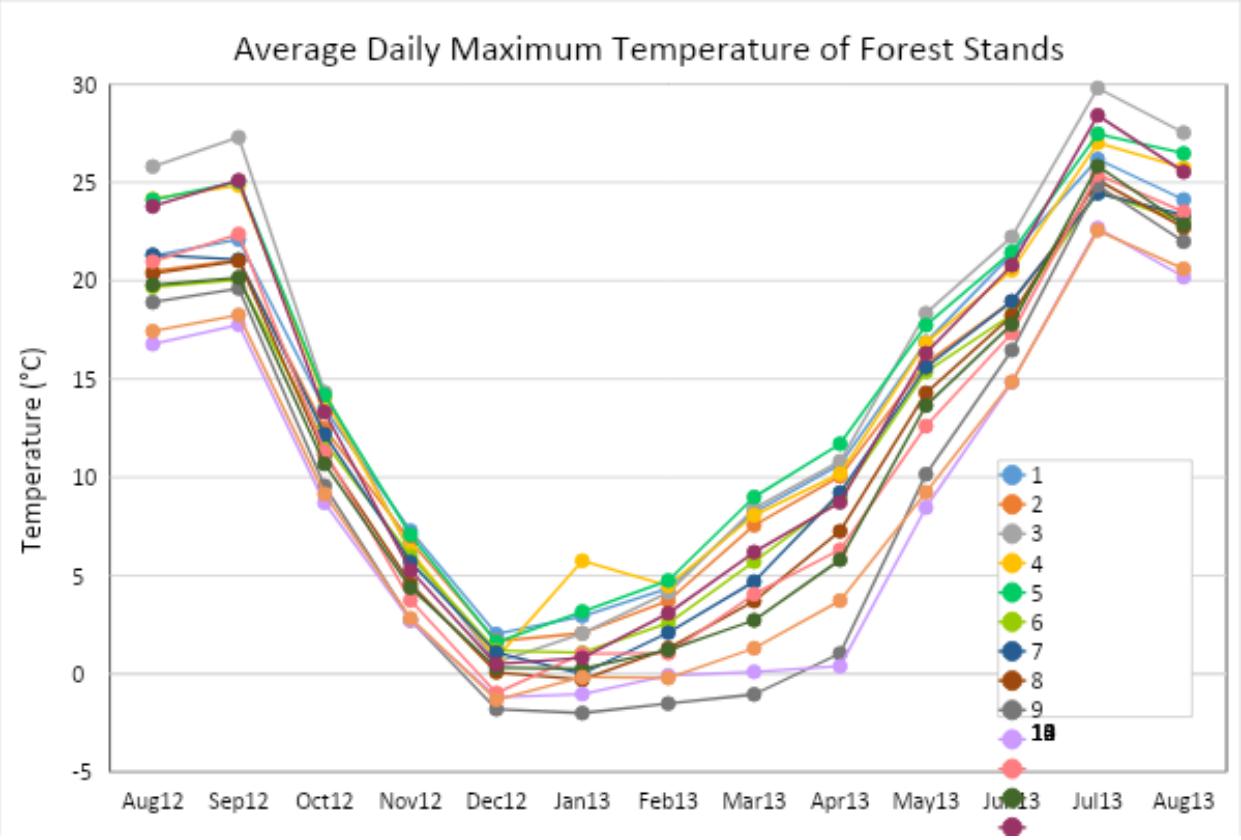

Figure 3. Monthly averages of daily maximum temperatures for 14 forest stands in the Gifford Pinchot National Forest, recorded from August 20, 2012, to August 16, 2013.

Monthly averages of daily maximum measured temperatures range from 2°C in winter to nearly 30°C during summer. The variability in monthly average temperature among stands also changed seasonally, with summer temperature ranges as large as 10°C, and winter variance less than 4°C. It also follows that the temperature anomaly between clearcut terrain and mature forest was generally smallest in winter. Average temperature of young, regrowth stands was more than 5°C higher than average

temperature of old growth stands in summer, and this temperature anomaly decreased to less than 1°C in the coldest month.

Shade Fraction

Shade fraction was calculated from the SMA of Landsat imagery, using the deep water endmember divided by the sum of all unmixed spectra as a proxy for shade (Figure 4). Relative shade fraction represents succession of stand densities and forest canopy structures between clearcut or young, regrowth terrain and mature, old-growth forests.

The white areas in Figure 4 signify regions of low shade and low forest density, and the darker areas signify relative increases in the amount of shade and higher forest density. Since the shade fraction implies relative shade, values stretched from 0 to 1 represent <5% shade to >80% shade. Shade fraction calculations from SMA based on 2013 imagery display an exponential relationship with 2008 stand density index values based on measured forest stand characteristics (Figure 5). This correlation is somewhat weaker than the 2008 shade fraction values in Roth (2009), which is attributed to temporal changes that may have occurred in stand density since the time of that study. Relative shade fraction of stands compared with stand density are difficult to determine due to clustering of values

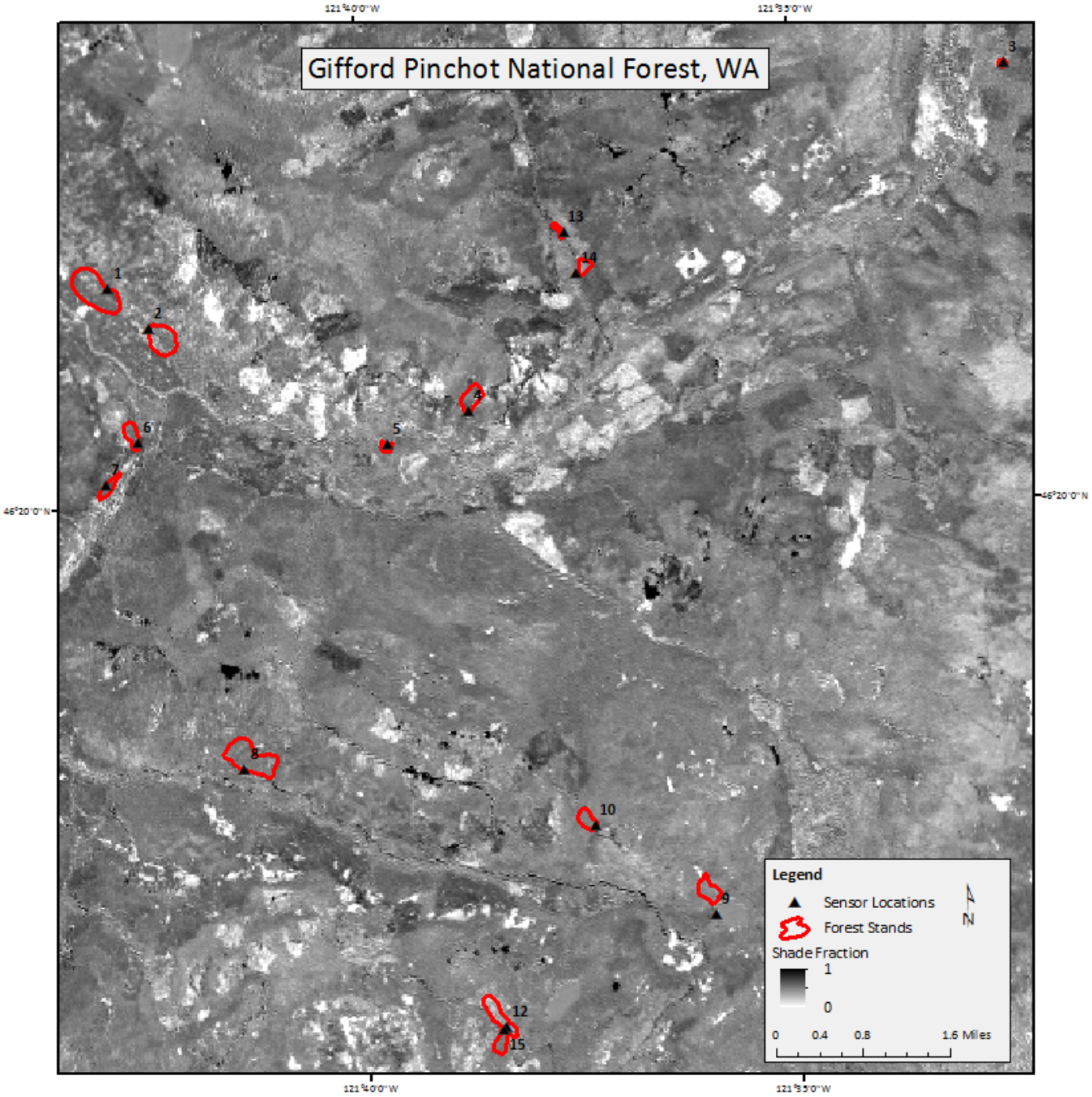

Figure 4. Shade fraction map for the study region. Forest stands and sensor locations are labeled by site. White regions represent areas with low shade, typically bare rock or clearcuts, and black regions represent areas with high shade, such as water. The gradient of gray represents relative shade, encompassing most forested terrain. Light gray corresponds with young regrowth sites, and mature forests are dark gray.

Stand 15 has the highest stand density index, while it has only the fourth highest shade fraction. Shade fraction values were normalized to between 0 and 1, and this normalization may be responsible for these deviations. Stand 13 has a shade fraction of 1 that is disproportionately assigned, while stand 15 has a slightly greater stand density index and shade fraction of just 0.64.

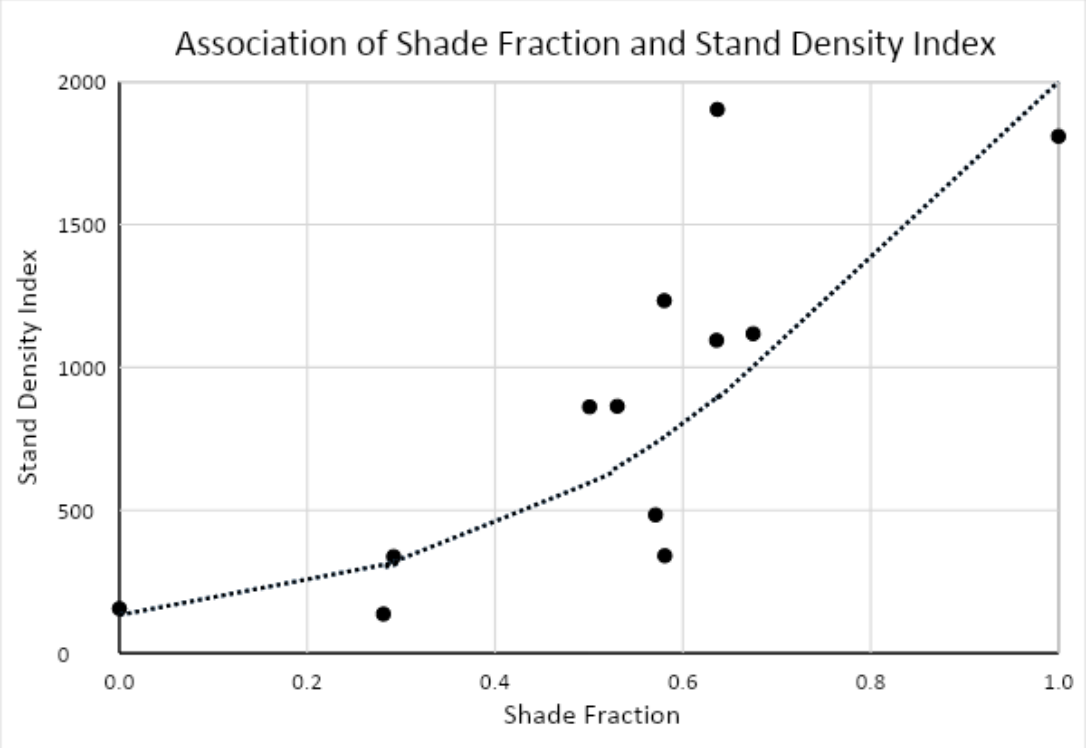

Figure 5. Shade fraction calculated from 2013 imagery versus 2008 stand density index values (Roth, 2009), labeled by site number.

Surface Temperature Model

The surface temperature model developed by O'Neal et al. (2010) and Roth (2009) was based on raw temperature measurements from late summer 2008. This model (equation 4) was applied to a full year of temperature fluctuations from August 2012 to August 2013, and performed

better than expected using the monthly averages of daily maximum temperatures. The model suitably predicted temperature throughout the study, with correlations ranging between 0.36 and 0.93 with the best environmental lapse rate, and a mean correlation of 0.69 for the year. Actual measured temperature was best predicted for the winter months where temperature variation among stands was generally small (1.29°C to 2.92°C anomalies for November through January). Figure 6a shows the high predictive power of maximum daily surface temperature for our study area for December 2012. The model also performed well in summer, with moderate predictive power shown by the coefficient of determination (r^2) in Figure 6b for June 2013.

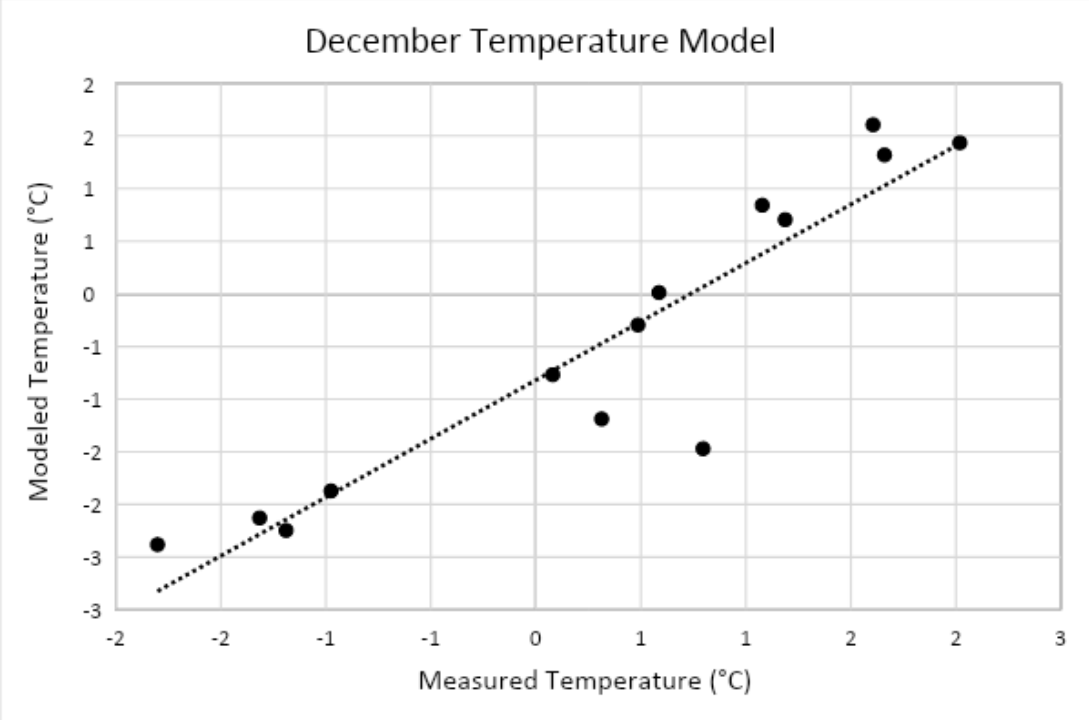

Figure 6a. Measured monthly average daily maximum temperature data versus modeled temperature values for December 2012, which had the highest correlation.

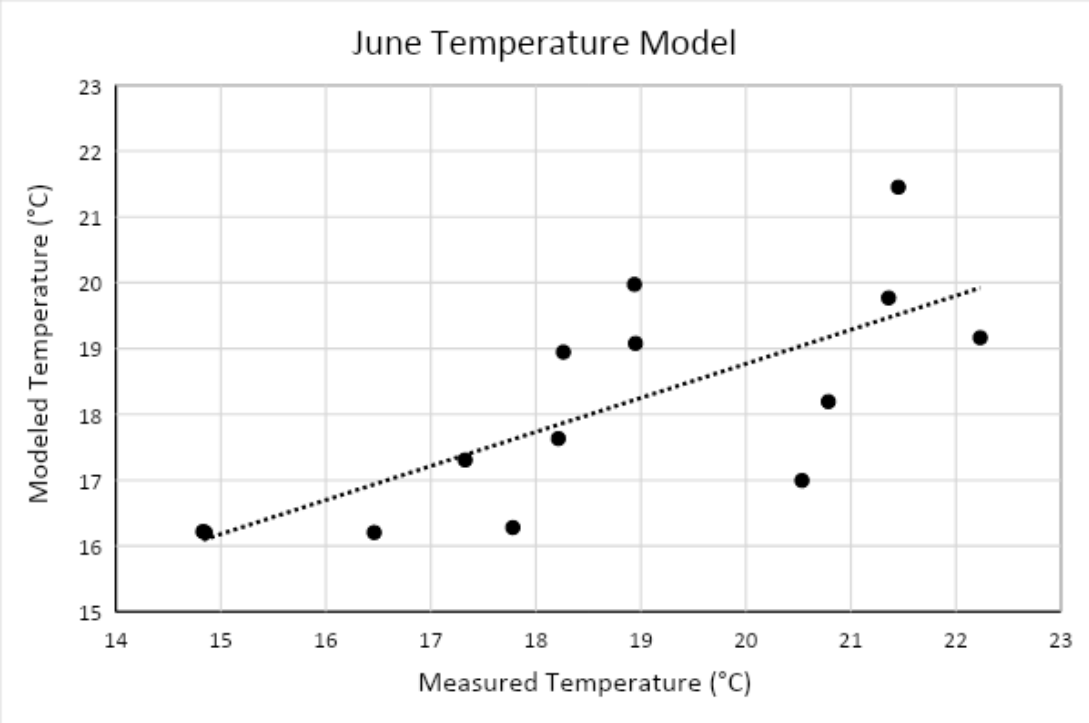

Figure 6b. Measured monthly average daily maximum temperature data versus modeled temperature values for June 2013.

Optimal lapse rate for the surface temperature model was evaluated on a monthly and annual basis. The model was run iteratively for environmental lapse rates between 0.001°/m and 0.01°C /m, and the most appropriate lapse rates were determined by maximizing correlation and minimizing root mean square error (RMSE) (Figure 6).

The best-fit environmental lapse rate was 0.0055°C/m, or 5.5°C/km, determined by minimizing the RMSE when applied to lapse rate iterations for year as a whole. This value is consistent with previous models, which used environmental lapse rates of 0.004°C/m and 0.007°C/m to best describe

measured temperature data at differing elevations (Roth, 2009; O'Neal et al., 2009).

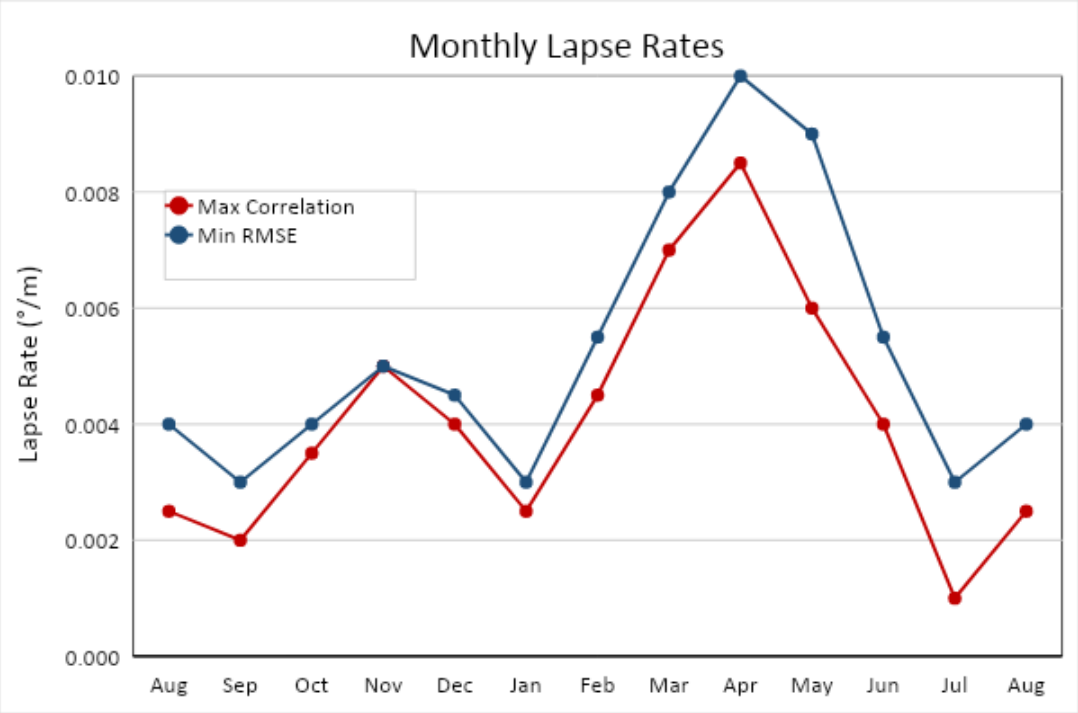

Figure 7. Best environmental lapse rates for each month, determined from maximum correlation and minimum RMSE.

Pre-Anthropogenic Model

The difference in shade fraction between the pre-anthropogenic modeled values and modern image suggests a proportional decrease of 0.25 in shade under present conditions. This translated to an average temperature increase of 0.94°C throughout the year, ranging from an increase in 0.33°C during winter months up to 1.58°C during summer. Figure 8 shows changes in increased modern-day temperature throughout the year, with largest differences in temperature during spring.

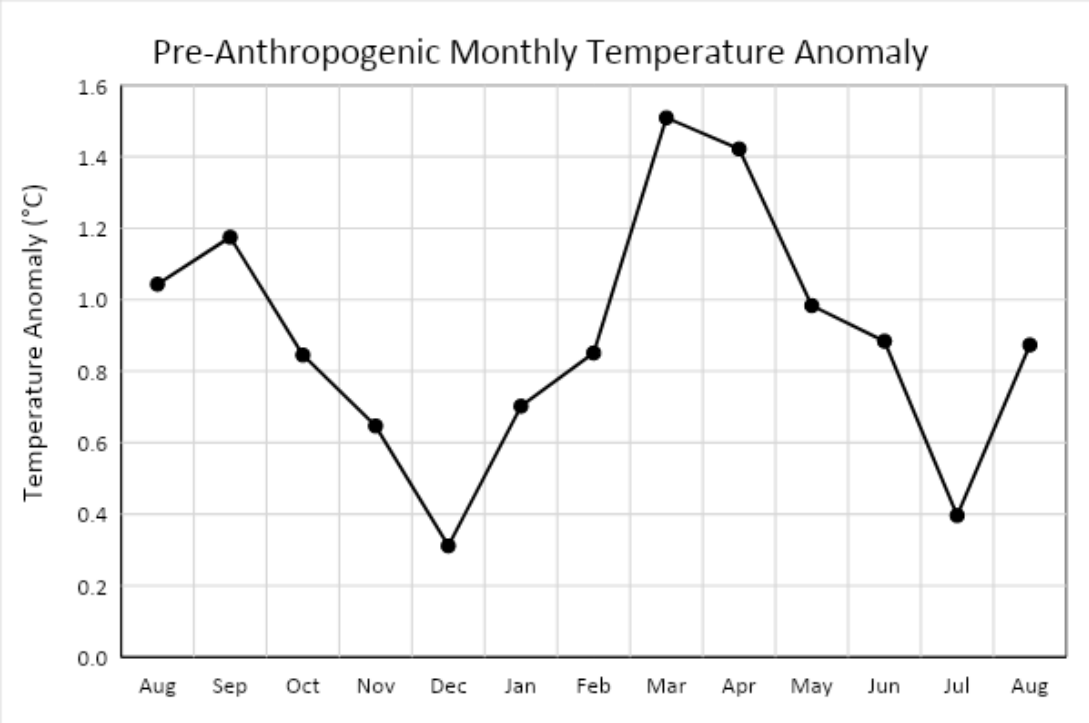

Figure 8. Temperature anomaly showing increase of present-day average monthly temperature from pre-anthropogenic temperature based on presence of vegetation from NDVI and shade fraction calculation.

The temperature difference was greatest in summer and spring, and least in winter, much like the surface temperature model. Temperature increased by between 0°C and 3.18°C during August (Figure 9), which is higher than the 0.7°C increase observed by O'Neal et al. (2010) for the study area during their summer data collection. For December, when the temperature anomaly was least, our model shows a temperature increase of 0.37°C to 0.95°C from the pre-anthropogenic to modern landscapes over this study area.

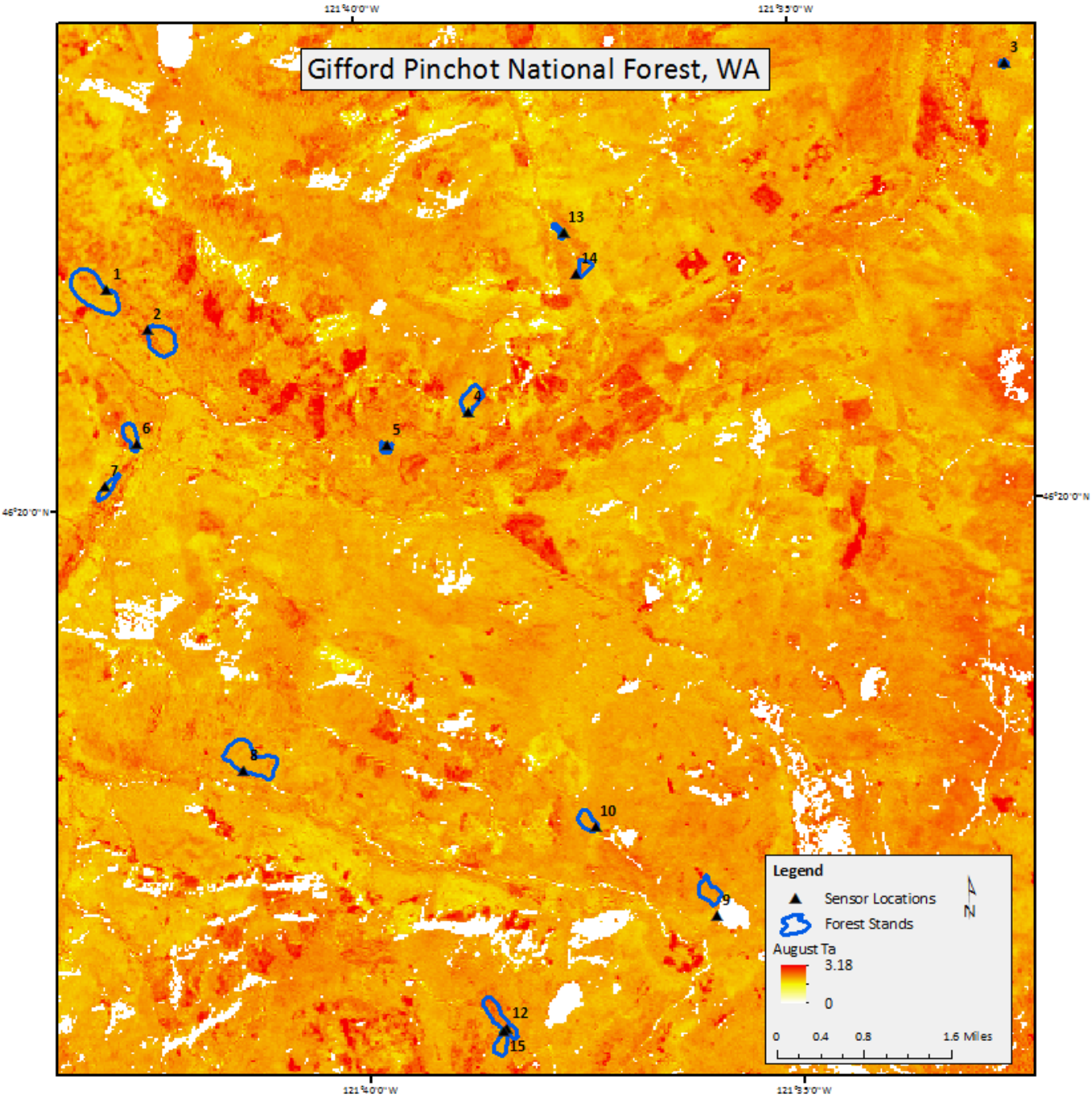

Figure 9. The August temperature anomaly shows an increase of present-day average monthly temperature from pre-anthropogenic temperature to between 0°C and 3.18°C. Greater temperature increases are associated with areas that have sparse vegetation such as clearcut or young regrowth stands.

Discussion

The data presented in this study validates that the shade-based temperature model can reasonably predict monthly average daytime temperature values and is improved by modeling seasonal fluctuations throughout the year. Using lapse rates and temperature anomalies that varied by month, we were able to provide a better fit model for predicting near-surface air temperature with changing elevations and stand densities. Correlation between stand-density index values and the modeled shade fraction were high ($r = 0.83$), indicating that shade fraction provides an accurate representation for stand height and density.

The association between overall mean temperature and elevation suggests that environmental lapse rate is an important predictor for modeling temperature, and this study found that 5.5°C/km was most appropriate. A lapse rate of 7°C/km is widely used for alpine settings (O'Neal et al., 2009); however, Roth (2009) found a smaller rate for summer temperatures of 4°C/km in the same study area.

Forest cover sheds latent and sensible heat, and has an overall cooling effect for tropical regions, as well as temperate regions during summer. By contrast, deforested areas in boreal regions are more efficient at shedding heat due to the strong albedo effect from snow cover. The alpine forests in the Cascades can be considered temperate or northern transitional, so I

anticipated that deforested areas during winter would have a similar cooling effect as with boreal regions.

The surface temperature model worked best for the winter months when temperature variation was lowest, which is surprising considering this model was originally developed for summer months without confidence that the model would be transferable to annual temperature cycles. This corresponds with the increased influence of the albedo effect on snow-covered clearcut terrain compared with mature forests. However, the albedo effect turned out to be minimal, since for the most part mature forests had lower daytime temperatures than clearcut areas throughout the winter. It is possible that these trends are reversed for nighttime or even average daily temperatures during winter.

Nearly all of topographic shade was removed the original satellite imagery. However, some unresolved shade remained in the stacked base layer before SMA, so a small error may have been carried on to the unmixed spectra used to calculate shade fraction. O'Neal et al. (2010) suggest that the presence of topographic shadows in the shade fraction image would result in an overrepresentation of mature forests from artificially high canopy densities, which would underestimate land cover change. This may have lowered the modeled temperature difference between the pre-anthropogenic and modern landscapes.

Our pre-anthropogenic model indicates that modern annual temperatures have increased by an average of 0.9°C throughout the year, compared with 0.7°C found by Roth (2009). The presence of topographic shade in that study may have led to underestimating the temperature anomaly. Added seasonal variations in this study's model, which was strongest in winter, also suggests a larger annual temperature anomaly, ranging from 0.3°C to 1.6°C throughout the year. The climatic response to pervasive logging in the northwest suggests the presence of a dominant regional forcing sufficient to influence glacier retreat.

Areas for Further Research

By studying how temperature increases or decreases throughout the year with canopy density, it is possible to evaluate how land cover changes contribute to anthropogenic climate forcing. Deforestation significantly alters the surface energy balance and temperature of alpine environments. It would be interesting to evaluate this surface temperature model on a multiple year timeline to examine how the extreme drought conditions observed over the last decade relate to canopy density. Further research on the albedo effect from seasonal snow cover would be helpful for determining average-annual climatic effects, as well as, any potential changes in the influence of albedo in conjunction with warming over the last decade. This information could help with decision making for land use and forestry management, as well as larger climate policies going into the future.

Acknowledgements

I would like to thank Michael O'Neal and Brian Hanson of the University of Delaware, who let me get my feet wet by participating in their field program in Washington in 2008 for support of Lyndsey Roth's master's thesis. I want to acknowledge Michael O'Neal for his time and assistance with remote sensing techniques during his sabbatical, and Brian Hanson for his invaluable expertise in climate modeling and scripting. I also want to thank Cameron Jasper and my family for their continual patience and support.

References

Barg, A. K. & Edmonds, R. L. (1999). Influence of partial cutting on site microclimate, soil nitrogen dynamics, and microbial biomass in Douglas-fir stands in western Washington. *Canadian Journal of Forest Research-Revue Canadienne De Recherche Forestiere, 29*, 705-713.

Bonan, G. B. (1997). Effects of land use on the climate of the United States. *Climatic Change, 37*, 449-486.

Bonan, G. B. (2008). Forests and climate change: Forcings, feedbacks, and the climate benefits of forests. *Science, 320*, 1444-1449.

Carlson, D. W. & Groot, A. (1997). Microclimate of clear-cut, forest interior, and small openings in trembling aspen forest. *Agricultural and Forest Meteorology, 87*, 313-329.

Fritts, H. C. (1961). An analysis of maximum summer temperatures inside and outside a forest. *Ecology, 42*, 436-440.

Goldstein, A. J. (2008). Temperature Response to 20th Century Landcover Change, and Its Influence on Recent Glacier Retreat. M.S. thesis, Department of Geography, University of Denver.

Gu, D. & Gillespie, A. (1998). Topographic Normalization of Landsat TM Images of Forest Based on Subpixel Sun-Canopy-Sensor Geometry. *Remote Sensing of Environment, 64*, 166-175.

Heithecker, T. D., & Halpern, C. B. (2006). Variation in microclimate associated with dispersed-retention harvests in coniferous forests of western Washington.

Hornbeck, J. W. (1970). Radiant energy budget of clearcut forested sites in West Virginia. *Forest Science, 16*, 139-145.

Houspanossian, J., Nosetto, M., & Jobbagy, E. G. (2013). Radiation budget changes with dry forest clearing in temperate Argentina. *Global Change Biology, 19*(4), 1211-1222.

Kane, V. R., Gillespie, A. R., McGaughey, R., Lutz, J. A., Ceder, K., & Franklin, J. F. (2008). Interpretation and topographic compensation of conifer canopy self-shadowing. *Remote Sensing of Environment, 112*, 3820-3832.

Klingaman, N. P., Butke, J., Leathers, D. J., Brinson, K. R., & Nickl, E. (2008). Mesoscale Simulations of the Land Surface Effects of Historical Logging in a Moist Continental Climate Regime. *Journal of Applied Meteorology and Climatology, 47*, 2166-2182.

Lee, X., Goulden, M. L., Hollinger, D. Y., Barr, A., Black, T. A., Bohrer, G., Bracho, R., Drake, B., Goldstein, A., Gu, L., Katul, G., Kolb, T., Law, B. E., Margolis, H., Meyers, T., Monson, R., Munger, W., Oren, R., Paw U, K. T., Richardson, A. D., Schmid, H. P., Staebler, R., Wofsy, S., & Zhao, L. (2011). Observed increase in local cooling effect of deforestation at higher latitudes. *Nature, 479*, 384-387.

Li, Y., Zhao, M., Motesharrei, S., Mu, Q., Kalnay, E., & Li, S. (2015). Local cooling and warming effects of forest based on satellite observations. *Nature Communications, 6*(6603), 1-8.

Little, E. L., Jr. (1980). A Practical Approach to Density Management. *Forestry Chronicle, 61*, 23-27.

McCaughey, J. H. (1985). A radiation and energy-balance study of mature forest and clearcut sites. *Boundary-Layer Meteorology, 32*, 1-24.

NOAA National Centers for Environmental Information, State of the Climate: Global Analysis for Annual 2015. Published January 2016, Accessed February 18, 2016. https://www.ncdc.noaa.gov/sotc/global/201513/.

O'Neal, M. A., Hanson, B., Leathers, D. J., & Goldstein, A. (2009). Estimating landcover-induced increases in daytime summer temperatures near Mt. Adams, Washington. *Physical Geography, 30*, 130-143.

O'Neal, M. A., Roth, L. B., Hanson, B., & Leathers, D. J. (2010). A Field-Based Model of the Effects of Landcover Changes on Daytime Summer Temperatures in the North Cascades. *Physical Geography*, *31*(2), 137-155.

Pearson, G. (1914). A meteorological study of parks and timbered areas in the western yellow pine forests of Arizona and New Mexico. *Monthly Weather Review, 41*, 1615-1629.

Roth, L. B. (2009). Modelling Landcover-Induced Increases in Daytime Summer Temperatures near Mount Adams, Washington. M.S. thesis, Department of Geography, University of Delaware.

USDA (1999). Gifford Pinchot National Forest – Vegetation. USDA Forest Service, Vancouver, WA.

Zhang, M., Lee, X., Yu, G., Han, S., Wang, H., Yan, J., Zhang, Y., Li, Y., Ohta, Y., Hirano, T., Kim, J., Yoshifuji, N., & Wang, W. (2014). Response of surface air temperature to small-scale land clearing across latitudes. *Environmental Research Letters, 9*, 2-7.